

Binarity and the abundance discrepancy problem in planetary nebulae

Romano L.M. Corradi, Jorge García-Rojas, David Jones, and Pablo Rodríguez-Gil

Instituto de Astrofísica de Canarias, E-38200 La Laguna, Tenerife, Spain

Departamento de Astrofísica, Universidad de La Laguna, E-38206 La Laguna, Tenerife, Spain

ABSTRACT

The discrepancy between abundances computed using optical recombination lines (ORLs) and collisionally excited lines (CELs) is a major unresolved problem in nebular astrophysics. We show here that *the largest abundance discrepancies are reached in planetary nebulae with close binary central stars*. This is illustrated by deep spectroscopy of three nebulae with a post common-envelope (CE) binary star. Abell 46 and Ou5 have O^{2+}/H^+ abundance discrepancy factors larger than 50, and as high as 300 in the inner regions of Abell 46. Abell 63 has a smaller discrepancy factor around 10, but still above the typical values in ionized nebulae. Our spectroscopic analysis supports previous conclusions that, in addition to “standard” hot ($T_e \sim 10^4$ K) gas, a colder ($T_e \sim 10^3$ K) ionized component that is highly enriched in heavy elements also exists. These nebulae have low ionized masses, between 10^{-3} and $10^{-1} M_\odot$ depending on the adopted electron densities and temperatures. Since the much more massive red-giant envelope is expected to be entirely ejected in the CE phase, the currently observed nebulae would be produced much later, in post-CE mass loss episodes when the envelope has already dispersed. These observations add constraints to the abundance discrepancy problem. Possible explanations are revised. Some are naturally linked to binarity, such as for instance high-metallicity nova ejecta, but it is difficult at this stage to depict an evolutionary scenario consistent with all the observed properties. The hypothesis that these nebulae are the result of tidal destruction, accretion and ejection of Jupiter-like planets is also introduced.

Subject headings: planetary nebulae: individual (A 46, A 63, Ou5) – ISM: abundances - binaries: close – novae, cataclysmic variables – planet–star interactions

1. Introduction

This work deals with two apparently unrelated, main topics in the study of planetary nebulae (PNe).

The first one is the role of binary evolution, which is the favoured explanation of the diverse morphologies displayed by PNe (e.g. Soker 1997; Balick & Frank 2002), but which may even be the cause of their mere existence (Moe & De Marco 2001; Soker 2006).

The second issue is the so-called *abundance discrepancy problem*. It is well known (see e.g. Osterbrock & Ferland 2006) that in photoionized nebulae – both PNe and H II regions – optical

recombination lines (ORLs) provide abundance values that are systematically larger than those obtained using collisionally excited lines (CELs). This a long-standing problem in nebular astrophysics, and has obvious implications on the measurement of the chemical content of the Universe, often done using CELs from emission regions and the ISM. The *abundance discrepancy factor* (*adf*) between ORLs and CELs is usually between 1.5 and 3 (see e.g. García-Rojas & Esteban 2007; Liu 2012; Esteban et al. 2014), but in PNe it has a significant tail extending to much larger values. The nebula with the largest known *adf* (~ 70 , Liu et al. 2006) is Hf 2–2, which has a close binary central star (Lutz et al. 1998).

In our recent study of the new Galactic PN IPHASXJ211420.0+434136 (Ou5), which also has a binary central star (Corradi et al. 2014), we noticed the unusual strength of recombination lines such as C II 4267 Å and the 4650 Å O II+N III blend. This points to large *adf* values also in this object, as well as in other binary PNe such as Abell 46 (Bond 1980) and Abell 63 (Bond, Liller & Mannery 1978) in which strong C II emission was detected (Pollacco & Bell 1997). The short orbital periods, between 8 and 11 hours, indicate that the central stars of these PNe have gone through a common-envelope (CE) phase in their previous evolution. Therefore, we decided to obtain deep spectroscopy of these three nebulae to investigate whether the abundance discrepancy problem in PNe is in some way related to the binary nature of their central stars. That this is indeed true is demonstrated by the results presented in the following.

2. Observations

H α +N II images of A 46 and A 63 were retrieved from the archives of the Isaac Newton Group of Telescopes and ESO. The image of A 46 is an 1-hr exposure from the 2.5m Isaac Newton Telescope on La Palma obtained in 2008 with the Wide Field Camera (pixel size 0''.33). Seeing was 1''.0 FWHM. The image of A 63 was obtained in 1995 at the 3.5m ESO/NTT with EMMI (exposure time 30 min, pixel size 0''.27, seeing 0''.9). The image of Ou5 is the one described in Corradi et al. (2014). The inner regions of the nebulae are displayed in Figure 1.

Spectra of A 46, A 63 and Ou5 were obtained on August 16–18 2014 with the 4.2m WHT telescope and the double-arm ISIS spectrograph. The long slit of ISIS was opened to 1'' width and positioned through the brightest parts of the nebulae as indicated in Figure 1 and in Table 1. In the blue arm of ISIS, grating R1200B was used, providing a dispersion of 0.22 Å pix⁻¹ and a resolution of 0.8 Å. In the red arm, grating R316R gave a dispersion of 0.92 Å pix⁻¹, and a resolution of 3.4 Å. Two different grating tilts were adopted in different nights in order to have a global wavelength coverage from 3610 to 5050 Å in the blue, and from 5400 to 9150 Å in the red, with little vignetting at the wavelength ends. The spatial

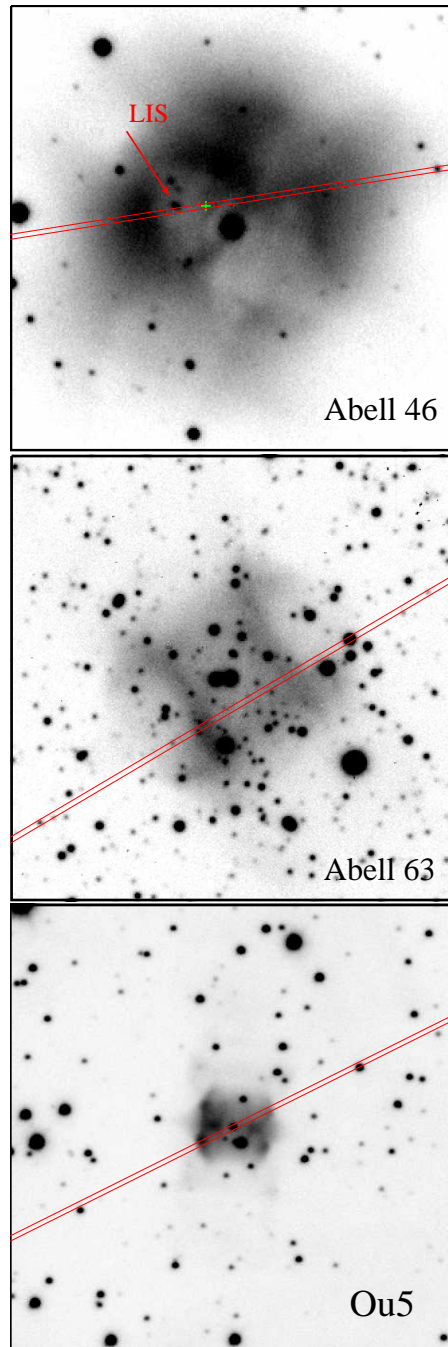


Fig. 1.— H α +N II images of the nebulae. The field of view is 90'' \times 90'' in all frames. The location of the long slit is shown. In A 46, the green cross indicates where emission of recombination lines peaks along the slit. The position of the LIS identified in the nebula is also indicated.

scale was $0''.2 \text{ pix}^{-1}$ in the blue, and $0''.22 \text{ pix}^{-1}$ in the red. Depending on the wavelength setting, total exposure times were of 2 hours for A 46, 2 to 3.3 hours for A 63, and 2 to 4.7 hours for Ou5. The spectrophotometric standards BD+28 4211, BD+33 2642, and Feige 110 from Oke (1990), and HR 718 from Hamuy et al. (1994) were observed for flux calibration. Seeing varied significantly during observations, and only data obtained with a seeing value $\leq 1''.6$ FWHM were retained. Images and spectra were reduced using packages *ccdred* and *twodspec* in IRAF¹.

3. Data analysis

To increase the signal from these low surface brightness nebulae, 1-D spectra were extracted by integrating all the nebular emission included in the long slit. Note that in A 46, at the position indicated by the arrow in Figure 1, the slit intersects an elongated knot. In the spectra, this feature clearly stands out for its strong [N II] 6548,6583, [S II] 6716,6731, and more moderate [O II] 3726,3729 emission relative to the surrounding nebula, from which it seems to be blue-shifted by $\approx 10 \text{ km s}^{-1}$. It could be a low-ionization small-scale structure (LIS) as often found in PNe (Gonçalves, Corradi, & Mampaso 2001). Other similar blobs are seen in the image, but it should also be noted that the field is also rich in small background galaxies. This feature does not affect the following analysis, and is not considered any further in this work.

Figure 2 shows an illustrative portion of the spectra of the nebulae, in a wavelength range where some of the most relevant ORLs and CELs are located. Emission-line fluxes were measured by means of multi-Gaussian fit using *splot*. Both in the blue and red, fluxes measured in the two spectrograph settings were rescaled using the emission lines in the overlapping spectral range. The flux differences in these overlapping lines (after scaling) were used to estimate the errors in the flux measurement. Identification of the observed lines, their fluxes and errors are presented in Table 2. All line fluxes are normalised to $H\beta=100$,

where the observed $H\beta$ flux integrated along the slit is 3.53×10^{-14} , 1.80×10^{-14} , and $1.37 \times 10^{-14} \text{ erg cm}^{-2} \text{ s}^{-1}$ for A 46, A 63, and Ou5, respectively.

The nebular reddening was computed from the hydrogen line ratios, specifically the Balmer $H\alpha$, $H\beta$, $H\gamma$, and $H\delta$ lines and the Paschen 10–3, 11–3 and 12–3 transitions. The reddening law of Fitzpatrick (2004) was adopted. The theoretical hydrogen line ratios have a small but non-negligible dependence on the electron density and temperature n_e and T_e . As discussed below, in addition to a standard nebular component at $T_e \sim 10^4 \text{ K}$, in these nebulae there is evidence for a much colder component at $\approx 10^3 \text{ K}$, as for instance indicated by the Balmer jump in A 46 (Sect. 4). We therefore computed the reddening by adopting either $T_e=12500 \text{ K}$, characteristic of the CELs, or $T_e=1000 \text{ K}$, as suggested by the ORLs indicators. The mean values of the logarithmic extinction at $H\beta$ of each nebula ($c(H\beta)$) are listed in Table 3 for both temperature assumptions. Those derived using the CELs temperature are 0.17 dex larger, and in good agreement with the previous estimates by Pollacco & Bell (1997) and Corradi et al. (2014), as expected considering that they were determined under the same assumption. In the case of A 46, they are also consistent with the reddening maps of Schlegel et al. (1998), which indicate a total foreground dust column corresponding to $c(H\beta)=0.17$. In the following, we conservatively use the $c(H\beta)$ values determined with the CELs temperature to deredden the observed line fluxes, as the ORLs temperature are more uncertain, especially for A 63 and Ou5. However, we also repeated the whole analysis with the lower $c(H\beta)$ values resulting from the ORLs temperature. Differences in the results are small and do not affect our conclusions. Errors on the dereddened fluxes includes the contribution of the uncertainty in the $c(H\beta)$ value.

4. Physical and chemical properties of the nebulae

4.1. Physical conditions

The physical conditions for our nebulae were computed using several emission-line ratios. The electron temperatures, T_e , and electron densities, n_e , are presented in Table 3. The computa-

¹IRAF is distributed by the National Optical Astronomy Observatory, which is operated by the Association of Universities for Research in Astronomy (AURA) under cooperative agreement with the National Science Foundation.

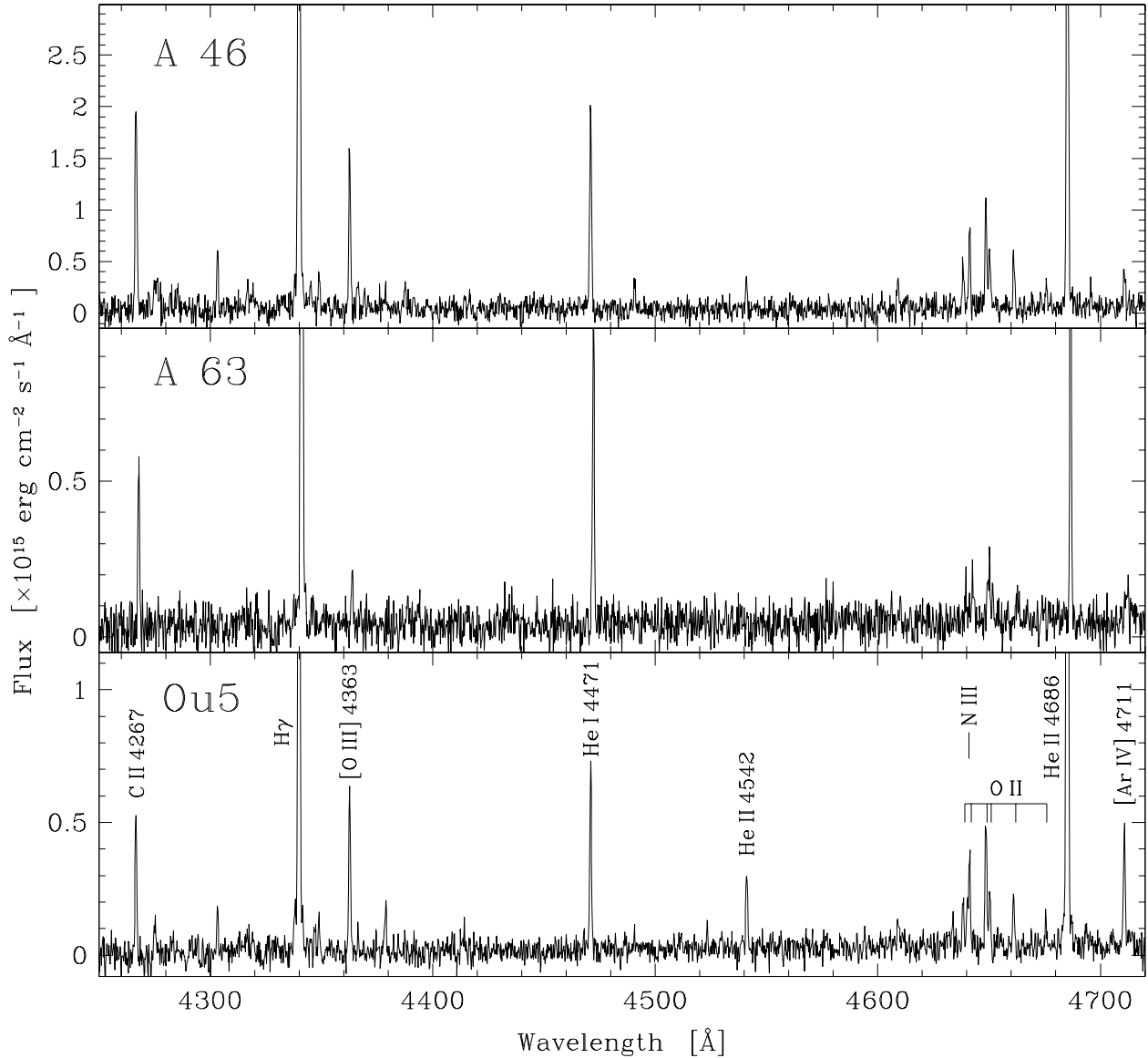


Fig. 2.— Illustrative portion of the spectra of the nebulae integrated along the slit.

tions of physical conditions were done with PyNeb (Luridiana et al. 2014), a python based package that allows derivation of the physical conditions and ionic and elemental abundances from emission lines. The methodology followed for the derivation of n_e and T_e has been described in García-Rojas et al. (2012). We used the state-of-the-art atomic data listed in Table 4. Errors in these diagnostics were computed via Monte Carlo simulations.

We computed $n_e([\text{O II}])$ and $n_e([\text{S II}])$ for the three nebulae, and with lower precision $n_e([\text{Ar IV}])$ for A 46 and Ou5. Similarly to what found by Liu et al. (2006) for Hf 2–2, we find that $n_e([\text{O II}])$ is significantly higher than $n_e([\text{S II}])$ and $n_e([\text{Ar IV}])$. For the following analysis, we adopted the weighted average of $n_e([\text{O II}])$ and $n_e([\text{S II}])$ for A 46 and A 63, and of $n_e([\text{O II}])$, $n_e([\text{S II}])$ and $n_e([\text{Ar IV}])$ for Ou5. Note that the main results are almost independent on the assumed n_e .

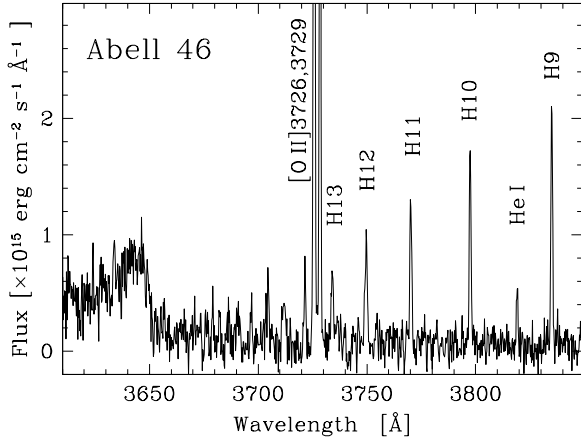


Fig. 3.— Spectrum of A 46 at the Balmer jump.

The intensity of the auroral [N II] $\lambda 5755$ line and the trans-auroral [O II] $\lambda\lambda 7320+30$ lines were corrected for the contribution of recombination using equations (1) and (2) in Liu et al. (2000). A preliminary calculation of the N^{2+}/H^+ and O^{2+}/H^+ abundance ratios by means of N II multiplet 3 and O II multiplet 1 was used to compute the recombination contribution to [N II] $\lambda 5755$ and [O II] $\lambda\lambda 7320+30$, respectively. This resulted (Table 6) in relatively small corrections for the [N II] line flux, but very large corrections for the [O II] line fluxes. This means that T_e from the corresponding temperature diagnostics would be lower than computed neglecting recombination. In particular, the fact that recombination dominates the trans-auroral [O II] emission (100% in A 46 and Ou5, and 56% in A 63), no reliable T_e estimation can be derived using these lines. $T_e([N II])$ is also very uncertain owing to the large errors in the measurement of the faint [N II] $\lambda 5755$ and multiplet 3 N II lines.

Given the relatively high ionization degree of our three objects, we also computed the contribution of recombination to the auroral [O III] $\lambda 4363$ line using equation (3) in Liu et al. (2000). To estimate the O^{3+}/H^+ ratio, we assumed

$$O^{3+}/H^+ = (He/He^+)^{2/3} \times (O^+/H^+ + O^{2+}/H^+).$$

Using He^+/H^+ , He^{2+}/H^+ , and O^{2+}/H^+ ratios from ORLs (see Table 7), and O^+/H^+ from ORLs in Ou5 and from CELs rescaled to ORLs using O^+/O^{2+} CELs ratio for A 46 and A 63 (see Table 7), the contribution to [O III] $\lambda 4363$ is estimated

to be between $\sim 14\%$ and $\sim 43\%$ depending on the nebula for the slit-integrated spectra (Table 6, but see also discussion in Section 4.3). The values obtained for T_e with and without recombination correction are summarized in Table 3. Owing to the large uncertainties in $T_e([N II])$ and $T_e([O II])$, and considering the overall high excitation of the nebulae, we finally adopted $T_e([O III])$ as representative of the whole nebula, (see Table 3 and discussion below).

To test whether in these nebulae part of the ORLs emission comes from a cold, high-metallicity gas component (e.g. Liu et al. 2006), we also checked some T_e diagnostics from ORLs. Unfortunately, the most widely used diagnostics, that is the ratio between the Balmer discontinuity at 3646 \AA and the Balmer decrement ratio, could only be measured in A 46 (Figure 3). In this nebula, the Balmer continuum temperature (in K) was determined following the equation by Liu et al. (2001):

$$T(\text{Bac}) = 368 \times (1 + 0.259y^+ + 3.409y^{2+}) \left(\frac{\text{Bac}}{\text{H11}} \right)^{-3/2}$$

where y^+ and y^{2+} are the He^+/H^+ and He^{2+}/H^+ ratios respectively, and $\text{Bac}/\text{H11}$ is the ratio of the discontinuity of the Balmer jump in $\text{erg cm}^{-2} \text{s}^{-1} \text{\AA}^{-1}$ to the H I H11 line flux. For A 46, a very low $T_e(\text{Bac}) = 1150 \pm 550$ K, is obtained. We also considered other T_e line diagnostics from recombination lines, such as T_e derived from He I line ratios ($T_e(\text{He I } 5876/4471, 6678/4471)$, Zhang et al. 2005; Liu et al. 2006) and T_e derived from the ratio of O II ORLs to [O III] CELs ($T_e(\text{O II } V1/F1)$, Peimbert et al. 2014). Additionally, for A 46 we could measure the T_e sensitive ratio O II 4089/4649 (Wesson, Liu, & Barlow 2003). As it can be seen in Table 3, all these diagnostics give values of the electron temperature that are much lower than those derived from CELs diagnostics. All this clearly points to the presence of a nebular component of cold ionized gas where most of the ORL emission arise, as it has been claimed by e.g. Liu et al. (2006).

4.2. Chemical abundances

Ionic chemical abundances from CELs were computed using PyNeb (Luridiana et al. 2014) and the atomic data in Table 4. Errors in the

line fluxes and the physical conditions were propagated via Monte Carlo simulations. The average n_e and $T_e([\text{O III}])$ for the whole nebula computed in the previous section were used. Assuming other density values (e.g. the one measured for a specific ion) would cause very small changes on the majority of ions, with the exception of O^+ , S^+ , Cl^{2+} and Ar^{3+} , whose abundances have a more marked dependence on n_e . However, even so the main conclusions of this work would not change. Ionic abundances are presented in Table 7.

As with recombination lines, He^+ and He^{2+} abundances were computed from the He I 4471, 5876, 6678 Å and He II 4684 Å lines using the updated atomic data in Table 5. In our spectra, we detected and measured several heavy element ORLs, mainly of O II and C II, but also of O I. To compute O^{2+}/H^+ ratio we used multiplet 1 O II ORLs around 4650 Å, which are the brightest and widely used O II ORLs (see e. g. García-Rojas et al. 2013, and references therein). We also computed the C^{2+}/H^+ ratio using C II at 4267 Å; this is a $3d - 4f$ transition that is, in principle, purely excited by recombination. The sources of the recombination coefficients that we have used to compute the ionic abundances of C^{2+} and O^{2+} are listed in Table 5. Tsamis et al. (2003) and Ruiz et al. (2003) pointed out that the upper levels of the transitions of multiplet 1 of O II are not in local thermodynamic equilibrium (LTE) for densities $n_e < 10^4 \text{ cm}^{-3}$, which is the case for our three objects, and the abundances derived from each individual line may differ by factors as large as four. To recover the correct abundances for individual lines, we applied the non-LTE corrections estimated by Peimbert et al. (2005) to our data. We also computed the O^{2+}/H^+ ratio from the sum of all lines of the multiplet following the recipe given by Esteban et al. (1998). This method takes into account the intensity of the whole multiplet and is not affected by non-LTE effects. This is the value that we finally adopt as representative of the O^{2+}/H^+ ORLs abundance ratio (Table 7).

Additionally, we computed the n_e that minimizes the dispersion of individual abundances obtained from the O II multiplet 1 lines. This quantity, labelled as $n_e(\text{O II})$, is shown in Table 3. For A 46 and A 63, $n_e(\text{O II})$ is very similar to $n_e([\text{O II}])$. In Ou5, $n_e(\text{O II})$ is higher than electron densities derived from CELs, in agreement with what found

in Hf 2–2 by Liu et al. (2006).

Finally, in Ou5 we also computed the O^+/H^+ ORLs ratio (see Table 7), as we detected an emission line that we identify as the blend of three O I ORLs at $\sim 7772 \text{ Å}$ (see Tab 2). These lines are hardly detected in deep emission spectra of other PNe and H II regions, mainly because they are intrinsically faint and frequently blended with strong telluric emission lines (which is not the case in the spectrum of Ou5).

The O^{2+} *adf* was computed for each object from the comparison of the ORLs and CELs ionic abundances. In Ou5, we could also compute the *adf* for O^+ . Results are shown in Table 7. It is clear that the *adfs* of these nebulae— and especially in A 46 and Ou5— are very large, independently of adopting or not a correction for recombination in the calculation of T_e . A detailed discussion on the possible origins of the large *adfs* of these objects, the largest ones found in PNe and two orders of magnitude larger than in H II regions, is presented in Sect. 6.

4.2.1. Total abundances

Total abundances for N, C, O, Ne, S, Ar and Cl were computed using the ionization corrections factors (ICFs) published by Delgado-Inglada, Morisset & Stasińska (2014) from a large grid of photoionization models of PNe. The He abundance was computed by simply adding the He^+ and He^{2+} abundances. Total abundances are presented in Table 8.

4.3. Spatial variations

The low surface brightness of these nebulae does not allow us to study in detail spatial variations of the chemical abundances and *adfs*. Useful insights can however be gained by inspecting the spatial distribution of selected CELs and ORLs along the spectrograph slit. They are presented in Figs. 4 and 5 for A 46 and Ou5. To decrease the noise in the faintest emission lines, profiles were smoothed with a boxcar average of 5 pixels ($1''$) width for A 46, and 3 pixels ($0''.6$) for Ou5. Profiles have been arbitrarily scaled in flux to plot all lines using the same display. A 63 is not shown because of the low S/N of several of these lines.

In the light of $\text{H}\alpha$ (Figure 1), A 46 looks amorphous and diffuse. Even so, its brightest regions seem to trace the outline of a low surface bright-

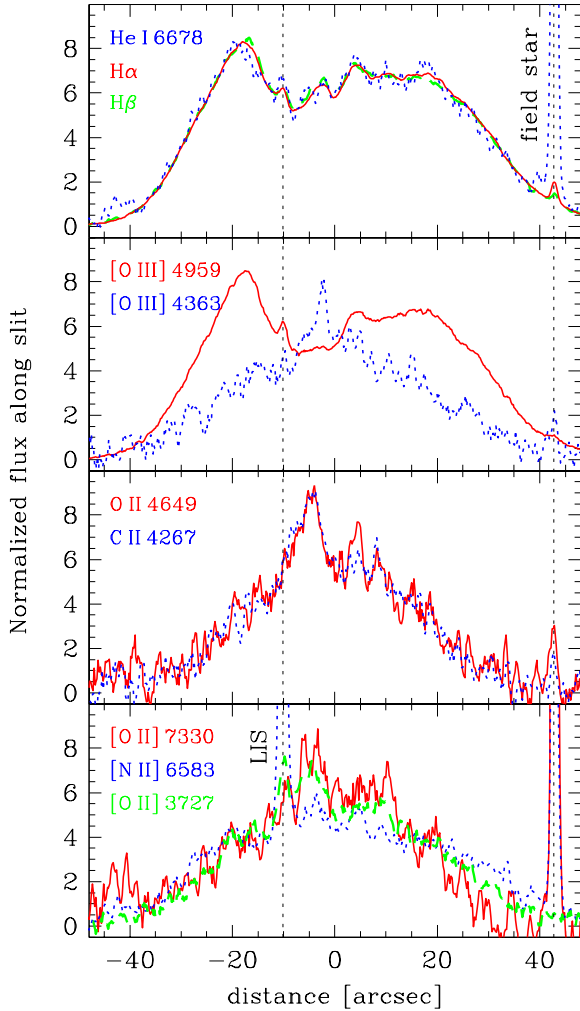


Fig. 4.— Spatial profiles along the slit of selected emission lines for A 46. The x -axis zero point corresponds to the part of the slit closest to the central star. The emission peak for the ORLs C II and O II lines is marked in Figure 1.

ness inner “cavity” with a bipolar shape whose long axis is approximately oriented at position angle P.A.= 45° . Figure 4 shows that H I, He I and strong CELs such as [O III] 4959 have a similar spatial distribution that follows what is seen in Figure 1. On the other hand, the ORLs emission, illustrated by C II 4267 and O II 4649, peaks in the innermost regions, inside the low surface brightness H α “cavity”. Their peak is indicated by a green cross in Figure 1. This central enhancement is a standard characteristic of the ORLs abun-

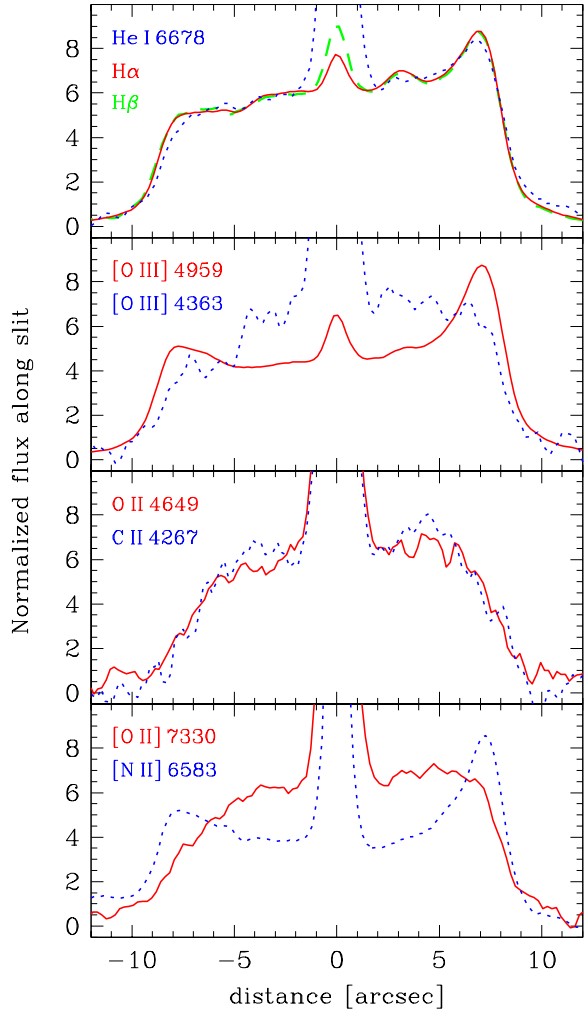


Fig. 5.— Same as in Figure 4, but for Ou5. The central peak is the continuum emission from the central star. The [O II] 3727 profile is not shown here because of the significant, asymmetrical contamination of the background Galactic emission.

dances (Liu 2003; Tsamis et al. 2008). Most of the fluctuations observed in the ORLs spatial profiles are noise in these faint lines, which prevents the detection of small-scale spatial variations such as for instance done by Tsamis et al. (2008) in NGC 7009. More puzzling is the behaviour of the auroral line [O III] 4363, which shows a very similar spatial distribution to the ORLs, even if its peak is displaced to the west by a couple of arcseconds. The marked difference between the [O III] 4959 and [O III] 4363 spatial profiles apparently indicates

that $T_e([\text{O III}])$ decreases from 20000 K in the innermost regions to 11000 K in the outer parts. However, in the previous section we have shown that auroral lines can be significantly affected by recombination. Table 6 provides some crude estimates for the integrated spectrum, but the actual contribution of recombination to each line as a function of position can only be roughly estimated with the present data. The spatial profile of $[\text{O III}] \lambda 7330$, whose emission should be dominated by recombination, is also very similar to that of the ORLs and qualitatively supports the hypothesis that at least part of the apparent $T_e([\text{O III}])$ radial gradient could be spuriously produced by variable contribution of recombination to the auroral lines.

This is confirmed by the following exercise. We extracted the spectrum within 7 arcsec of the ORLs peak in the spatial profiles of A 46. Even if some line fluxes are one order of magnitude smaller than in the integrated spectra, most of the critical lines could be measured. By proceeding as for the integrated spectra, 48% of the $[\text{O III}] \lambda 4363$ flux is estimated to be produced by recombination and was corrected accordingly. The value $T_e([\text{O III}]) = 17800 \pm 1900$ K that would be obtained by neglecting recombination is then lowered to 12950 ± 1150 K when it is instead taken into account. A $T_e(\text{O II } \lambda 6583)$ of 3840 ± 200 K is computed, which is only slightly lower than for the integrated spectrum. Densities are about twice as high, namely $n_e([\text{S II}]) = 560^{+2200}_{-450} \text{ cm}^{-3}$ and $n_e([\text{O II}]) = 5750^{+6000}_{-2950} \text{ cm}^{-3}$. Total abundances determined from CELs only vary slightly compared to those found using the integrated spectrum. But, as far as the O^{2+} abundance is concerned, the CELs abundance slightly decreases to 7.70 ± 0.11 while the ORL one more markedly increases to $10.21^{+0.17}_{-0.19}$. This results in an *adf*(O^{2+}) over 300 in the inner regions of A 46!

Ou5, which has a clean bipolar geometry (Corradi et al. 2014), shows similar results (Figure 5). H I, He I, $[\text{O III}] \lambda 4959$, and $[\text{N II}] \lambda 6583$ have a similar spatial distribution, peaking at the limb-brightened edges of the bipolar lobes. On the other hand, ORLs such as C II and O II, as well as the auroral lines of $[\text{O III}]$ and $[\text{O II}]$ are more concentrated toward the center, and are mutually similar. Therefore recombination should be carefully considered when the auroral lines are used to

determine the physico-chemical conditions in this kind of nebulae.

5. Total H α flux and nebular mass

A 63 and Ou5 were observed by the IPHAS H α photometric survey of the Galactic plane (Drew et al. 2005). Therefore their IPHAS H α + $[\text{N II}]$ images can be flux calibrated using the information in the IPHAS Second Data Release (Barentsen et al. 2014). The observed, total H α fluxes of these nebulae, after removing the contribution of $[\text{N II}] \lambda 6583$ to the IPHAS H α filter using our spectroscopy, are listed in Table 1. Errors are of the order of 10%. Taking advantage of the fact that the image of A 46 in Figure 1 was obtained with the same instrumentation and filter in a clear night, we adopted the mean value of the zeropoint of the IPHAS survey to also calibrate this image. The additional error introduced by this assumption is another 10%.

With the total H α flux and the physical parameters determined from spectroscopy, and adopting the distances quoted in Table 1, the nebular ionized mass can be estimated. The total ionized mass of hydrogen was computed by applying the expression:

$$m_{\text{neb}}(H^+) = \frac{4\pi D^2 F(\text{H}\beta) m_p}{h\nu_{\text{H}\beta} n_e \alpha_{\text{H}\beta}^{\text{eff}}(H^0, T_e)}$$

where $F(\text{H}\beta)$ is the dereddened H β flux, D is the distance to the object, m_p is the proton mass, n_e is the electron density, $h\nu_{\text{H}\beta}$ is the energy of an H β photon and, finally, $\alpha_{\text{H}\beta}^{\text{eff}}(H^0, T_e)$ is the effective recombination coefficient of H β . The usual dependence on the square of the distance appears in the formula. In this respect, it should be noted that the distances of A 46 and A 63 were originally computed through the stellar parameters of the central binaries, which should provide more reliable determinations than any statistical method, especially when the peculiar nature of these nebulae is considered.

As $\alpha_{\text{H}\beta}^{\text{eff}}(H^0, T_e) \propto T_e^{-1}$, the total mass is roughly proportional to the adopted electron temperature T_e and inversely proportional to the electron density n_e . The dual-component nature of these nebulae prevents a precise mass determination, as the relative amounts of H I emitting at the low T_e indicated by the Balmer jump and the

He I or O II ORLs, and that emitting at the much higher CELs T_e is not known. Strictly speaking, at least for A 46 one would be tempted to consistently adopt for hydrogen the temperature computed using the Balmer jump, namely 1000 K. As with densities, there is also a clear difference (by up to a factor of 8) between those computed from [O II] and those computed from [S II]. Assuming $T_e=1000$ K and the average n_e from CELs, we determine an H^+ mass of 1×10^{-3} , 5×10^{-4} , and $5\times 10^{-3} M_\odot$ for A 46, A 63, and Ou5, respectively.

However, even if the total amount of metals in the hot and cold gas phases is comparable as for instance estimated for Hf 2-2 (Liu et al. 2006), the much higher metallicity of the cold component implies that the majority of hydrogen must be in the hot component. It seems therefore reasonable to adopt $T_e([O III])$, which would imply H^+ masses almost one order of magnitude larger, namely 8×10^{-3} , 4×10^{-3} , and $5\times 10^{-2} M_\odot$ for A 46, A 63, and Ou5, respectively.

Finally, in the less likely case that all hydrogen comes from a plasma with $T_e([O III])$ and the lowest electron density measured ($n_e([S II])$), we obtain 4×10^{-2} , 1×10^{-2} , and $2\times 10^{-1} M_\odot$, respectively. These should be just taken as conservative upper limits to the total amount of H^+ in these nebulae (for the adopted distances). Liu et al. (2006) found a similarly low H^+ mass of $1.4\times 10^{-2} M_\odot$ for Hf 2-2.

Therefore, in spite of the large uncertainties in these calculations, the clear conclusion is that these nebulae with large *adfs* and close binary central stars have a very small total ionized mass, one or more orders of magnitudes lower than typical of Galactic PNe (see e.g. Pottasch 1984). The total nebular mass could in principle be larger if part of it is in neutral/molecular form. However, spectral indicators such as the absence of [O I] 6300 emission (Harman & Seaton 1966; Kaler & Jacoby 1989), which is thought to be produced at the interface between ionized and neutral gas via charge exchange reactions, point to optically thin, density bounded nebulae.

6. Discussion

Two of the three PNe that we studied, namely A 46 and Ou5, have abundance discrepancy factors that are among the largest ones found in

PNe. In particular, A 46 has the largest *adf* ever measured, with the exception of the hydrogen-deficient knots that are directly observed in Abell 30 (Wesson, Liu, & Barlow 2003). Our third target, A 63, has a lower *adf* (~ 10), but still above the average value in PNe.

Our three target PNe have close binary central stars with orbital periods around ten hours. Therefore these observations, together with the additional case of Hf 2-2 (Liu et al. 2006), reveal a clear connection between the most extreme representatives of the abundance discrepancy problem and the binarity of the central sources. The above-mentioned Abell 30 (and the morphologically similar Abell 58 aka V605 Aquilae, which experienced a nova-like outburst in 1905) were also proposed to contain a close binary (Wesson et al. 2008), but no direct evidence has been found yet.

Our spectroscopic analysis supports the previous interpretation that two different gas phases coexist in these nebulae (e.g. Liu et al. 2006; Tsamis et al. 2008): hot gas at 10^4 K with standard metallicity where the CELs can be efficiently excited, and a much cooler (10^3 K) plasma with a highly enhanced content of heavy element abundances (which cause the cooling) where only ORLs form. How much each component contributes to the total mass, and how they are distributed and mixed, is poorly known, because existing data are not able to spatially resolve them. One common characteristic, also shared by the nebulae studied in this work, is that the ORLs emission is enhanced in the central regions of the nebulae, where the *adf* reaches a value over 300 in A 46. Liu et al. (2006) estimated that similar amounts of metals are in the hot and cold gas of Hf 2-2, but the amount of H and He in each component cannot be determined. This prevents the calculation of precise X^{i+}/H^+ abundances for each gas phase individually (Liu et al. 2006), and therefore all values in Table 8 should be taken with caution. For instance, the large helium content that is measured in A 63 and Ou5 may not be completely real (see also Liu 2003; Tsamis et al. 2008). Only ionic abundance ratios, such as for example N^+/O^+ , are free of this bias. In this respect A 46, and to a lesser extent A 63 (because of its large errors) and Ou5², have low $N^+/O^+ \approx N/O$ CELs abundance

²The much lower N^+/O^+ ratio for this nebula computed by

ratios, typical of low-metallicity SMC PNe, or alternately indicating substantial oxygen enhancement compared to nitrogen. But even this ratio should be taken with caution, considering the high excitation of the nebulae. We have also noticed that CELs temperature gradients within a nebula can be at least partly spurious, caused by a varying contribution of recombination to the emission of the auroral lines. This additional uncertainty also affects the determination of the CELs abundances.

6.1. The nature of these nebulae and the implications for the abundance discrepancy problem

The main result of this work is that any explanation of the abundance discrepancy problem must include the fact that *the most pathological cases are planetary nebulae with a close binary central star*. This casts light on the origin of the problem. Let’s consider previously proposed and new scenarios, and their *pro et contra*.

A key point to understand the evolution of these systems is the small ionized mass of the nebulae (Sect. 5). Let’s take $10^{-2} M_{\odot}$ as a representative figure of the nebular mass for the systems that we have considered. The total mass in the high-metallicity component would then be a (likely small) fraction of it. These low masses dispute the usual interpretation of the origin of these nebulae. It is generally thought that PNe with close binary central stars went through a common-envelope phase when the radius of the primary star increased in the AGB phase and engulfed the companion. The CE interaction caused the shrinkage of the orbit to the current small separations ($\sim 2 R_{\odot}$ for the four objects in Table 1) and provoked the complete ejection of the envelope, forming the PN. However, the nebular masses that we have estimated are far too low compared to the AGB envelope masses expected for 0.5-0.6 M_{\odot} cores and standard initial-to-final mass relationships, even if some mass loss prior to the AGB is allowed (De Marco et al. 2011). The exercise has been done by Afsar & Ibanoglu (2008) and De Marco et al. (2011) for A 46 and A 63, for

which stellar parameters are known (Table 1). In De Marco et al. (2011), consistency between the stellar evolution and binary parameters is reached for CE masses of 0.4 M_{\odot} for A 46 and 1.2 M_{\odot} for A 63, i.e. one to three orders of magnitude larger, respectively, than what we measured. The similar or only slightly larger nebular masses of Ou5 and Hf 2-2 add strength to this conclusion, even if the stellar parameters for these two systems are not precisely known³. This missing-mass problem is even more severe considering that the whole CE is thought to be ejected in a very short timescale (\sim few years, see e.g. Sandquist et al. 1998), limiting the possibility that the PN is dispersed over a large volume.

As it is evident that the systems at some point went through a CE phase (given the present small orbital separation), the envelope of the primary star would have been ejected a long time ago and would have now vanished in the interstellar medium. Note that the 0.5 M_{\odot} mass of the central star of A 46 is at the limit between RGB and AGB core masses. It cannot be excluded that in this case (but can be ruled out for A 63 which has a typical AGB core mass of 0.63 M_{\odot}) the CE interaction, ejection, and orbital shrinking occurred in the RGB phase of the primary.

Then the currently observed low-mass nebulae would be produced much after the CE phase, in post-CE mass loss episodes when the massive AGB envelope has already dispersed. Even so, their central stars have to be still hot and luminous to be able to ionize the nebulae, as it is indeed observed (see e.g. Afsar & Ibanoglu 2008).

6.1.1. Very late thermal pulses (VLTPs)

This hypothesis has been discussed in several articles (Liu et al. 2006; Wesson et al. 2008). In general, thermal pulses in the post-AGB phase are expected to be relatively frequent (Blöcker 2001). In the best studied case, Sakurai’s object, the estimated ejected mass is $2 \times 10^{-3} M_{\odot}$ (Hajduk et al. 2005), i.e., in the possible range of what we have measured. Gas falling back from the ejected envelope, accreting on the post-AGB star, and perhaps triggering a VLTP was predicted and discussed by, e.g., Frankowski & Soker (2009). In those specific

Corradi et al. (2014) was caused by the use of the auroral [O II]7320,7730 lines, that we have shown here to be severely affected by recombination processes.

³For Ou5, they are very likely in the range of A 46 and A 63 (Corradi et al. 2015, in preparation).

calculations, however, the total amount of fallback material, 10^{-5} to $10^{-3} M_{\odot}$, seems on the low side of what we observed, and the timescale for accretion is too short to allow the massive, ejected CE to vanish completely.

The VLTP ejecta are expected to basically represent the intershell abundances, with $C/O \gg 1$. In the case of Ou5, the ORL C/O ratio could be estimated as $C/O = a (C^{2+}/O^{2+})$, where $a=1.12$ is the ICF from Delgado-Inglada, Morisset & Stasińska (2014) that could be consistently computed using the ORL O^+ and O^{2+} abundances. We obtain $C/O=0.55 \pm 0.24$ for this nebula. For A 46 and A 63, no ORL O^+ abundance determination is available, and therefore the ICF can only be estimated using CELs which would indicate values very close to unity. We obtain $C/O=0.78 \pm 0.11$ for A 46, and 1.66 ± 0.47 for A 63 which is the only nebula where the C/O ratio seems to be above unity. Therefore, in spite of the uncertainty involved in the use of the faint ORLs, the low C/O ratios estimated in A 46 and Ou5, as well as in Hf 2–2 (Liu et al. 2006), argue against VLTPs as the origin of the high-metallicity ejecta causing the large observed *adfs*.

6.1.2. Nova-like outbursts

Nova outbursts are natural phenomena in interacting binaries. They result from thermonuclear runaways on the surfaces of white dwarfs (WDs) accreting hydrogen-rich matter in binary systems (see e.g. Gehrz et al. 1998). Nova ejecta are metal enriched by mixing between the accreted envelope and the WD core. Therefore, in principle, the metal-rich gas in our target nebulae could be ejected in nova outbursts from the close binary central stars, as suggested by Wesson, Liu, & Barlow (2003) and Wesson et al. (2008) for A 30 and A 58. In these two cases, the hypothesis of a nova eruption could explain the large neon enrichment of their hydrogen-deficient knots, if produced in a massive ($M \geq 1.2 M_{\odot}$) ONeMg WDs. For A 58, this scenario (in combination with a final helium shell flash) or the alternative possibility of a stellar merger are evaluated in Lau, De Marco & Liu (2011).

However, there is no indication that mass transfer from the secondaries to the primaries is currently going on in the systems that we have studied, because the secondary stars – albeit inflated

– do not fill their Roche lobe (Afsar & Ibanoglu 2008). To feed the WD, accretion must therefore come from circumbinary material left-over in the systems from the CE phase. A possibility is that the envelope is not removed completely in the CE interaction and part of it remains gravitationally bounded to the system. The non-accreted part of this circumstellar gas, with normal AGB abundances, could then interact with the nova ejecta and partially mix with it producing the observed dual-component nebulae. In this respect, it should be noted that the existing simulations of the CE process fail to eject the entire envelope, a large fraction of which remains gravitationally bound to the system (Sandquist et al. 1998; Passy et al. 2012; Ricker & Tamm 2012). This may result in a series of CE and fall-back events, and in the formation of a left over, low mass circumbinary disk (Kashi & Soker 2011; Kuruwita 2015, Kuruwita, De Marco & Staff, in preparation), which could in turn form metal-rich dust as perhaps observed in the putative post-CE system V1309 Sco (Nicholls et al. 2013).

Possible problems are the very low mass of classical nova ejecta ($< 10^{-3} M_{\odot}$, but generally much smaller, see e.g. Gehrz et al. 1998), and the short timescale (a few years) of their nuclear burning and high luminosity phase that are needed to light up the PNe. Long-lasting outbursts at high WD luminosity can be achieved if the mass accretion rate is higher than in classical novae, as for instance occurs in symbiotic (very slow) novae. The relevant parameters space should be explored in detail to see how this hypothesis can fit our post-CE PNe (cf. e.g. Yaron et al. 2005).

An additional important parameter is the expansion velocity of the ejecta. In the PNe that we have studied, the ORL emitting gas phase does not show the large expansion velocities (few to many hundred km s^{-1}) typical of classical and symbiotic novae, which would be easily revealed at the resolution of our spectra. While more precise information is not available yet, a further constraint for the modeling is that both the hot and cold gas components have expansion velocities more typical of PNe than of novae.

6.1.3. Planetary material

A source of the metal-rich component in the nebulae might be planetary debris that survived

the CE phase. Indeed, about a quarter of *single* WDs have considerable amounts of metals in their photosphere, that are explained by accretion of tidally disrupted planetesimals/asteroids/comets that survived through all previous evolutionary phases of the star (see e.g. Farihi et al. 2014).

The possible contribution of solid bodies to the metal-rich component in PNe was first mentioned by Liu (2003) and then investigated by Henney & Stasińska (2010). They conclude that solid bodies could provide the source of the high-metallicity gas only if they are meter-sized or larger, their evaporation process extends back to the final AGB evolution, mixing with the gas component at “normal” AGB metallicity is inefficient, and systems possess a much more massive population of comets than is found in our Solar system.

Note also that Tsamis et al. (2011, 2013) and Mesa-Delgado et al. (2012) proposed that photo-evaporating protoplanetary disks are the cause of the smaller *adfs* found in H II regions.

6.1.4. Planets destruction

Another possibility is that these post-CE nebulae are produced by the destruction of one or more circumbinary Jovian planets. There is increasing evidence that post-CE planets exist (Parson et al. 2014; Zorotovic & Schreiber 2013; Bear & Soker 2014). It is therefore possible that planets in unstable orbits spiral in, are tidally disrupted, and collide with the post-AGB star (Bear & Soker 2012). The hydrogen-rich envelope of the planet would be stripped first, and then its metallic core. Part of this material would be accreted by the WD: at high accretion rates, the gas cannot be processed and inflates a red-giant envelope, producing a new CE phase and eventually the ejection of a new nebula with the dual nature (H-rich from the planet envelope and metal-rich from its core) that we have observed. The new CE would also favour the formation of highly bipolar nebulae such as Ou5 and A 63, by forcing the CE ejection toward the orbital plane, and/or producing jets from one of the two stars (as observed in A 63). A possible problem with this hypothesis is the apparently enhanced helium abundance of our target PNe (Table 8), which is not characteristic of planets. However, the He abundances in these high-*adf* objects are likely to be overestimated (Tsamis et al. 2008).

While this scenario should be taken as highly speculative at this stage, it has several positive aspects such as the fact that the process for planet collision is long enough ($>10^6$ year) to allow the CE to vanish, the ejection could be split into different phases (the planet’s atmosphere and core), and the observed nebular masses are in a plausible range corresponding to 1-10 Jupiter masses. In such case, Sir William Herschel would have been right in coining the name *planetary* nebulae!

6.2. Other implications and conclusions

If our hypothesis of an intimate relation between binarity and large *adfs* is correct, we predict that many – if not all – the PNe where large *adfs* have been measured are post-CE binaries. One already confirmed case is NGC 6778 which indeed contains a close binary with $P_{orb}=0.15$ (Miszalski et al. 2011). Other primary candidates to search for binarity are M 1-42, M 2-36, M 3-26, M 3-32, NGC 6153 and NGC 1501 (Liu 2003; Tsamis et al. 2004; Ercolano et al. 2004), as well as the already mentioned Abell 30 and Abell 58. Note that our conclusion does not imply the opposite hypothesis, i.e. that *all* post-CE PNe have large *adfs*. For example, NGC 5189 has a close binary central star (Manick, Miszalski & McBride 2015) but a low *adf* (García-Rojas et al. 2013). Also, no oxygen or carbon recombination lines are detected in relatively deep spectra of the Necklace binary PN (Corradi et al. 2011).

If some of the post-CE nebulae are not genuine AGB envelopes, but rather post-CE mass loss events or post-RGB systems, the total fraction of close binary PN central stars would be smaller than presently estimated ($\sim 15\%$ Miszalski et al. 2009), and perhaps more consonant with the fraction of main-sequence binaries (De Marco et al. 2013; Douchin et al. 2014, but also see Boffin 2014).

Concluding, we have added new ingredients to the discussion of the nature of PNe with close binary central stars, the CE evolution, and the abundance discrepancy problem. The main result of this work is the clear link between binary stellar evolution and the formation of high *adfs* in PNe. At the moment, none of the proposed scenarios to explain this result clearly stands out, but this is likely because observations provide still limited constraints. To further progress, a larger sample of

objects should be analyzed to highlight the basic relationships among the numerous parameters involved. In particular, more precise determinations of crucial quantities such as the nebular masses and chemical compositions for each (normal and enriched) nebular components, and the binary parameters (to better reconstruct the evolution of the systems), are needed.

Finally, even if the binary nature of the central stars seems to be an essential ingredient to understand the abundance discrepancy problem in PNe, it is hard to envisage its relevance to other astrophysical contexts such as H II regions. This may imply that different causes should be sought to fully understand this long-standing astrophysical problem, as proposed by García-Rojas & Esteban (2007). On the other hand, as discussed in the previous sections, some related phenomena may be involved, like for instance the possible contribution of protoplanetary disks in H II regions and of planetary debris in PNe.

This work is based on observations obtained with the 4.2m WHT and 2.5m INT telescopes of the Isaac Newton Group of Telescopes, operating on the island of La Palma at the Spanish Observatories of the Roque de Los Muchachos of the Instituto de Astrofísica de Canarias. The WHT spectra of 14 October 2014 were obtained in service time. Also based on data obtained from the ESO Science Archive Facility. We are extremely grateful to Noam Soker and Orsola De Marco for their significant contribution, in terms of original ideas and proper criticism, to the discussion in Sect. 6.1. We also thank Valentina Luridiana for her help with PyNeb, Grazyna Stasińska, Christophe Morisset, and César Esteban for a critical reading of the manuscript, and the referee for his/her very useful comments. This research has been supported by the Spanish Ministry of Economy and Competitiveness (MINECO) under grants AYA2012-35330, AYA2011-22614, and AYA2012-38700. JGR acknowledges support from Severo Ochoa excellence program (SEV-2011-0187) postdoctoral fellowship. PRG is supported by a Ramón y Cajal fellowship (RYC2010-05762).

Facilities: ING:Herschel (ISIS) ING:Newton (WFC) ESO:NTT (EMMI)

REFERENCES

- Afsar, M., & Ibanoglu, C. 2008, MNRAS, 391, 802
- Balick, B., & Frank, A. 2002, ARA&A, 40, 439
- Barentsen, G., Farnhill, H. J., Drew, J., et al. 2014, MNRAS, 444, 3230
- Bear, E., & Soker, N. 2012, ApJ, 749, L14
- Bear, E., & Soker, N. 2014, MNRAS, 444, 1698
- Bell, S. A., Pollacco, D. L., & Hilditch R. W. 1994, MNRAS, 270, 449
- Blöcker, T. 2001, Ap&SS, 275, 1
- Boffin, H. M. J. 2014, arXiv:1410.3132
- Bond, H. E. 1980, IAU Circ. 3480, 0
- Bond, H. E., Liller, W., & Mannery, E. J. 1978, ApJ, 223, 252
- Butler, K., & Zeppen, C. J. 1989, A&A, 208, 337
- Corradi, R.L.M., Sabin, L. Miszalski, B., et al. 2011, MNRAS, 410, 1349
- Corradi, R. L. M., Rodríguez-Gil, P., Jones, D., et al. 2014, MNRAS, 441, 2799
- Davey, A. R., Storey, P. J., & Kisielius, R. 2000, A&AS, 142, 85
- Delgado-Inglada, G., Morisset, B., & Stasińska, G. 2014, MNRAS, 440, 536
- De Marco, O., & Soker, N., 2002, PASP, 114, 796
- De Marco, O., Passy, J.-C., Maxwell, M., et al. 2011, MNRAS, 411, 2277
- De Marco, O., Passy, J.-C., Frew, D. J., Moe, M., & Jacoby, G. H. 2013, MNRAS, 428, 2118
- Douchin, D., De Marco, O., Frew, D.J., et al. 2014, in Asymmetrical Planetary Nebulae VI conference, Morisset C. Delgado-Inglada G. & Torres-Peimbert S. eds., id. 18 (online at www.astroscu.unam.mx/apn6/PROCEEDINGS)
- Drew, J., Greimel, R., Irwin, M. J., et al. 2005, MNRAS, 362, 753
- Ellis, D. G., & Martinson, I. 1984, Phys. Scr., 30, 255

- Ercolano, B., Wesson, R., Zhang, Y., et al. 2004, MNRAS, 354, 558
- Esteban, C., Peimbert, M., Torres-Peimbert, S., & Escalante, V. 1998, MNRAS, 295, 401
- Esteban, C., García-Rojas, J., Carigi, L., et al. 2014, MNRAS, 443, 624
- Fang, X., Storey, P. J., & Liu, X.-W. 2011, A&A, 530, A18
- Fang, X., Storey, P. J., & Liu, X.-W. 2013, A&A, 550, C2
- Farihi, J., Wyatt, M.C., Greaves, J.S., et al. 2014, MNRAS, 444, 1821
- Fitzpatrick, E. L. 2004, in “Astrophysics of Dust”, Witt A.N., Clayton G.C. & Draine B.T. eds., ASP Conf. Ser., Vol. 309, p. 33
- Frankowski, A., & Soker, N. 2009, New Astronomy, 14, 654
- Froese Fischer, C., & Tachiev, G. 2004, Atomic Data and Nuclear Data Tables, 87, 1
- Galavís, M. E., Mendoza, C., & Zeippen, C. J. 1995, A&AS, 111, 347
- Galavis M. E., Mendoza C., & Zeippen C. J. 1997, A&AS, 123, 159
- García-Rojas, J., & Esteban, C., 2007, ApJ, 670, 457
- García-Rojas, J., Peña, M., Morisset, C., Mesa-Delgado, A., & Ruiz, M. T. 2012, A&A, 538, A54
- García-Rojas, J., Peña, M., Morisset, C., Delgado-Inglada, G., Mesa-Delgado, A., & Ruiz, M. T. 2013, A&A, 558, A122
- Gehrz, R.D., Truran, J.W., Williams, R.E., Starfield, S. 1998, PASP, 110, 3
- Gonçalves, D. R., Corradi, R. L. M., & Mampaso, A. 2001, ApJ, 547, 302
- Hajduk, M., Zijlstra, A.A., Herwig, F. 2005, Science 308, 231
- Hamuy, M., Suntzeff, N. B., Heathcote, S. R., et al. 1994, PASP, 106, 566
- Harman, R. J., & Seaton, M. J. 1966, MNRAS, 132, 15
- Henney, W.J., & Stasińska, G. 2010, ApJ, 711, 881
- Kaler, J. B., & Jacoby, G. H. 1989, ApJ, 345, 871
- Kashi, A., & Soker, N. 2011, MNRAS, 417, 1466
- Kaufman, V., & Sugar, J. 1986, Journal of Physical and Chemical Reference Data, 15, 321
- Kisielius, R., Storey, P. J., Ferland, G. J., & Keenan, F. P. 2009, MNRAS, 397, 903
- Kuruwita, R. 2005, Master of Research Thesis, Macquarie University
- LaJohn, L., & Luke, T. M. 1993, Phys. Scr., 47, 542
- Lau, H. H. B., De Marco, O., & Liu, X.-W. 2011, MNRAS, 410, 1870
- Liu, X.-W. 2003, in Planetary Nebulae: their evolution and role in the Universe, IAU Symp. 209, Kwok, Dopita & Sutherland eds., p. 339
- Liu, X.-W. 2012, in IAU Symp. 283, Planetary Nebulae: An Eye to the Future, Manchado, A. Stanghellini, L., & Schönberner, D. eds., p. 131
- Liu, X.-W., Storey, P. J., Barlow, M. J., Danziger, I. J., Cohen, M., & Bryce, M. 2000, MNRAS, 312, 585
- Liu, X.-W., Barlow, M. J., Danziger, I. J., & Storey, P. J. 2001, MNRAS, 327, 141
- Liu, X.-W., Barlow, M.J., Zhang, Y., Bastin, R.J., Storey P.J., 2006 MNRAS, 368, 1959
- Luridiana, V., Morisset, C., & Shaw, R. A. 2015, A&A, 573, A42
- Lutz, J., Alves, D., Becker, A., et al. 1998, Bulletin of the American Astronomical Society, 30, 894
- Manick, R., Miszalski, B., Mc Bride, V. 2015, arXiv:1501.03373
- McLaughlin, B. M., & Bell, K. L. 2000, Journal of Physics B Atomic Molecular Physics, 33, 597
- Mendoza, C. 1983, in Flower D. R., ed., IAU Symp. 103, Planetary Nebulae p. 143

- Mendoza, C., & Zeppen, C. J. 1982a, MNRAS, 199, 1025
- Mendoza, C., & Zeppen, C. J. 1982b, MNRAS, 198, 127
- Mesa-Delgado, A., Núñez-Díaz, M., Esteban, C., et al. 2012, MNRAS, 426, 614
- Miszalski, B., Acker, A., Moffat, A.F.J., Parker, Q. A., Udalski, A. 2009, A&A, 496, 813
- Miszalski, B., Jones, D., Rodríguez-Gil, P., et al. 2011, A&A, 531, A158
- Moe, M., & De Marco, O. 2006, ApJ, 650, 916
- Nicholls, C. P., Melis C., Soszynski I., et al. 2013, MNRAS, 431, L33.
- Oke, J. B., 1990, AJ, 99, 1621
- Parson, S. G., Marsch, T. R., Bours, M. C. P., et al. 2014, MNRAS, 438, L91
- Passy, J.-C., De Marco, O., Fryer, C. L., et al. 2012, ApJ, 744, 52
- Peimbert, A., Peimbert, M., & Ruiz, M. T. 2005, ApJ, 634, 1056
- Peimbert, A., Peimbert, M., Delgado-Inglada, G., García-Rojas, J., & Peña, M. 2014, Rev. Mex. Astron. Astrofis., 50, 329
- Podobedova, L. I., Kelleher, D. E., & Wiese, W. L. 2009, Journal of Physical and Chemical Reference Data, 38, 171
- Pollacco, D.L., & Bell, S.A. 1997, MNRAS, 284, 32
- Porter, R. L., Ferland, G. J., Storey, P. J., & Dettisch, M. J. 2012, MNRAS, 425, L28
- Porter, R. L., Ferland, G. J., Storey, P. J., & Dettisch, M. J. 2013, MNRAS, 433, L89
- Pottasch, S.R. 1984, *'Planetary nebulae'*, D.Reidel, Dordrecht
- Ramsbottom C. A., & Bell K. L. 1997, Atomic Data and Nuclear Data Tables, 66, 65
- Ricker, P. M., & Tamm, R. E. 2012, ApJ, 746, 74
- Ruiz, M. T., Peimbert, A., Peimbert, M., & Esteban, C. 2003, ApJ, 595, 247
- Sandquist, E. L., Taam, R. E., Chen, X., Bodenheimer, P., & Burkert, A. 1998, ApJ, 500, 909
- Schaub, S. C., Bodman, E., & Hillwig, T. C. 2012, JSARA, 5, 2
- Schlegel, D. J., Finkbeiner, D. P., & Davis, M. 1998, ApJ, 500, 525
- Soker, N. 1997, ApJS, 112, 487
- Soker, N. 2006, ApJ, 645, L57
- Storey, P. J. 1994, A&A, 282, 999
- Storey, P. J., & Hummer, D. G. 1995, MNRAS, 272, 41
- Storey, P. J., & Zeppen, C. J. 2000, MNRAS, 312, 813
- Storey, P. J., Sochi, T., & Badnell, N. R. 2014, MNRAS, 441, 3028
- Tayal, S. S. 2011, ApJS, 195, 12
- Tayal, S. S., & Gupta G. P. 1999, ApJ, 526, 544
- Tayal, S. S., & Zatsarinny, O. 2010, ApJS, 188, 32
- Tsamis, Y. G., Barlow, M. J., Liu, X.-W., Danziger, I. J., & Storey, P. J. 2003, MNRAS, 338, 687
- Tsamis, Y. G., Barlow, M. J., Liu, X.-W., Storey, P. J., & Danziger, I. J. 2004, MNRAS, 353, 953
- Tsamis, Y. G., Walsh, J. R., Péquignot, D., et al. 2008, MNRAS, 386, 22
- Tsamis, Y. G., Walsh, J. R., Vílchez, J. M., & Péquignot, D. 2011, MNRAS, 412, 1367
- Tsamis, Y. G., Flores-Fajardo, N., Henney, W. J., Walsh, J. R., & Mesa-Delgado, A. 2013, MNRAS, 430, 3406
- Yaron, O., Prialnik, D., Shara, M. M., & Kovetz, A. 2005, ApJ, 623, 398
- Wesson, R., Liu, X.-W., & Barlow, M. J. 2003, MNRAS, 340, 253
- Wesson, R., Barlow, M. J., Liu, X.-W., et al. 2008, MNRAS, 383, 1639
- Zhang, Y., Liu, X.-W., Liu, Y., & Rubin, R. H. 2005, MNRAS, 358, 457

Zorotovic, M., & Schreiber, M. R. 2013, A&A, 549,
A95

This 2-column preprint was prepared with the AAS L^AT_EX
macros v5.2.

TABLE 1
BASIC PROPERTIES OF THE PNE, CENTRAL STARS, AND OBSERVATIONAL DETAILS.

Name	PN G	R.A. (J2000)	Dec	Slit P.A. (deg)	D (kpc)	P_{orb} (days)	m_{cs} (M_{\odot})	m_2 (M_{\odot})	i ($^{\circ}$)	$F(H\alpha)$ ($\text{erg cm}^{-2} \text{s}^{-1}$)	$m_{neb}(H^+)^a$ (M_{\odot})
Abell 46	055.4+16.0	18 31 18.29	+26 56 12.9	100	1.7	0.47	0.51	0.15	80	8.87×10^{-12}	10^{-3} to 10^{-2}
Abell 63	053.8-03.0	19 42 10.20	+17 05 14.4	300	2.4	0.46	0.63	0.29	87	2.29×10^{-12}	10^{-4} to 10^{-2}
Ou5	086.9-03.4	21 14 20.03	+43 41 36.0	297	5	0.36	$m_2/m_{cs} \approx 0.4?$		90	0.91×10^{-12}	10^{-3} to 10^{-1}
Hf 2-2	005.1-08.9	18 32 30.93	-28 43 20.5	...	4.25	0.40	25-55	...	$\approx 10^{-2}$

NOTE.—For the original sources of the orbital periods, see <http://www.drdjones.net/?q=node/6>. Distances, binary and stellar parameters for A 46 are from Bell, Pollacco & Hilditch (1994), for A 63 from Afsar & Ibanoglu (2008), and for Ou5 from Corradi et al. (2014, 2015 in preparation). Hf 2-2 is not directly analyzed in this paper, but it is shown here because is the other key target for discussion in Sect. 6. Its spectroscopic analysis was done by Liu et al. (2006), the quoted central star inclination is from Schaub, Bodman & Hillwig (2012).

^aFor the adopted distance (col. 6), and computed as described in Sect. 5.

TABLE 2
LINE IDENTIFICATIONS, OBSERVED FLUXES AND THEIR % ERRORS

λ_0 (Å)	Ion	Mult.	Abell 46		Abell 63		Ou5	
			F(λ)	Error (%)	F(λ)	Error (%)	F(λ)	Error (%)
3634.25	He I	28	1.21	16
3679.36	H I	H21	0.80	23
3682.81	H I	H20	0.67	26
3686.83	H I	H19	1.03	18
3691.56	H I	H18	1.51	14
3697.15	H I	H17	0.95	20
3703.86	H I	H16	2.56	10
3711.97	H I	H15	2.49	10
3721.83	[S III]	2F	2.02	11	2.42	31
3721.93	H I	H14	*	*	*	*
3726.03	[O II]	1F	23.91	6	11.01	11	26.01	8
3728.82	[O II]	1F	14.82	6	6.61	12	20.68	8
3734.37	H I	H13	2.20	10	2.97	18	3.16	25
3750.15	H I	H12	3.88	8	3.78	16	3.12	25
3770.63	H I	H11	4.35	7	3.64	16	4.17	19
3797.63	[S III]	2F	5.49	7	6.56	12	5.16	16
3797.90	H I	H10	*	*	*	*	*	*
3819.61	He I	22	1.39	14
3835.39	H I	H9	6.60	6	7.15	11	7.26	12
3868.75	[Ne III]	1F	39.43	5	25.37	9	74.32	6
3888.65	He I	2	22.66	5	22.78	9	22.17	7
3889.05	H I	H8	*	*	*	*	*	*
3964.73	He I	5	0.91	19
3967.46	[Ne III]	1F	12.61	5	7.33	10	21.00	7
3970.07	H I	H7	16.69	5	17.41	8	16.57	7
4009.26	He I	55	0.67	25
4026.21	He I	18	3.58	7	2.86	16	3.59	19
4068.60	[S II]	1F	4.38	6	4.30	16
4069.62	O II	10	1.69	24
4069.89	O II	10	*	*
4076.35	[S II]	1F	2.56	8	2.99	21
4078.84	O II	10	0.37	:
4085.11	O II	10	0.67	25
4089.29	O II	48	1.16	15
4097.22	O II	20	2.69	8	3.20	20
4101.74	H I	H6	26.32	4	25.87	7	26.43	6
4104.99	O II	20	0.65	25
4107.09	O II	62	0.50	32
4119.22	O II	20	1.20	15
4132.80	O II	19	0.65	25
4153.30	O II	19	1.12	16
4267.15	C II	6	6.45	4	3.99	11	5.11	12
4275.55	O II	67	1.12	15	1.52	35
4276.75	O II	67	0.99	17
4294.92	O II	54	0.56	28
4303.61	O II	65	1.57	11	0.93	37	1.60	32
4303.82	O II	53	*	*	*	*	*	*
4317.14	O II	2	0.56	28
4319.63	O II	2	1.04	:

TABLE 2—Continued

λ_0 (Å)	Ion	Mult.	Abell 46		Abell 63		Ou5	
			F(λ)	Error (%)	F(λ)	Error (%)	F(λ)	Error (%)
4340.47	H I	H5	47.34	3	48.15	5	49.45	4
4345.56	O II	2	0.46	33	1.10	:
4347.41	O II	2D-2D ₀	1.22	40
4349.43	O II	2	0.93	18	1.44	35
4363.21	[O III]	2F	4.88	5	1.07	32	6.33	9
4366.89	O II	2	0.90	18
4379.55	Ne II	60	1.84	27
4387.93	He I	51	0.71	22
4414.90	O II	5	0.35	:
4416.97	O II	5	0.44	34
4471.47	He I	14	6.49	4	6.43	7	6.27	9
4491.23	O II	86a	0.80	20
4541.59	He II	4.9	0.76	21	2.56	18
4609.44	O II	92a	0.91	17	0.91	:
4638.86	O II	1	1.24	13	0.59	:	1.51	28
4640.64	N III	2	1.30	32
4641.81	O II	1	2.19	8	0.94	32	2.68	17
4641.85	N III	2	*	*
4649.13	O II	1	3.14	6	0.75	:	3.81	12
4650.84	O II	1	1.81	9	0.53	:	1.80	24
4661.63	O II	1	1.51	11	1.89	23
4676.24	O II	1	0.72	21
4685.68	He II	3.4	26.41	1	6.83	6	71.11	1
4711.37	[Ar IV]	1F	1.25	13	1.19	26	3.61	12
4740.17	[Ar IV]	1F	0.93	17	2.73	16
4859.32	He II	4.8	1.97	8	3.75	11
4861.33	H I	H4	100.00	0	100.00	1	100.00	1
4921.93	He I	48	1.58	10	1.78	17	1.46	25
4958.91	[O III]	1F	119.93	1	85.47	1	184.58	1
5006.84	[O III]	1F	361.10	1	259.49	1	567.04	1
5411.52	He II	4.7	5.15	7
5517.71	[Cl III]	1F	0.70	37
5666.64	N II	3	0.54	:
5679.56	N II	3	0.66	21	0.51	:	0.85	29
5754.64	[N II]	3F	0.40	33	0.47	:	0.85	29
5875.64	He I	11	22.06	4	22.47	8	20.12	6
6312.10	[S III]	3F	1.00	21
6402.25	Ne I	1	0.44	:
6406.30	He II	5.15	*	*
6461.95	C II	17.04	0.51	25	0.54	34
6527.11	He II	5.14	0.45	39
6548.03	[N II]	1F	1.40	12	2.26	15	5.44	9
6562.82	H I	H3	318.63	7	347.18	11	323.61	8
6578.05	C II	2	0.63	21	0.40	:	0.64	29
6583.41	[N II]	1F	4.95	7	5.26	12	15.05	8
6678.15	He I	46	6.27	7	6.12	13	5.72	9
6683.20	He II	5.13	0.35	:
6716.47	[S II]	2F	1.42	12	0.60	32	4.32	10
6730.85	[S II]	2F	1.28	13	0.65	30	3.45	10

TABLE 2—*Continued*

λ_0 (Å)	Ion	Mult.	Abell 46		Abell 63		Ou5	
			F(λ)	Error (%)	F(λ)	Error (%)	F(λ)	Error (%)
6890.88	He II	5.12	0.35	:
7005.67	[Ar V]	3P-1D	0.24	:
7065.28	He I	10	2.06	10	2.30	16	1.79	14
7135.78	[Ar III]	1F	5.58	9	8.33	14	13.12	10
7177.50	He II	5.11	0.24	:	0.71	23
7231.34	C II	3	0.35	:
7236.42	C II	3	0.74	22
7237.17	C II	3	*	*
7281.35	He I	45	0.28	:
7318.92	[O II]	2F	1.58	18	3.26	12
7319.99	[O II]	2F	*	*	*	*
7329.66	[O II]	2F	2.74	10	1.24	20	2.73	12
7330.73	[O II]	2F	*	*	*	*	*	*
7530.54	[Cl IV]	1F	0.32	:
7530.57	C II	16.08	*	*
7592.74	He II	5.10	1.04	17
7751.10	[Ar III]	2F	2.76	13
7771.93	O I	1	1.00	18
7774.17	O I	1	*	*
7775.39	O I	1	*	*
8045.63	[Cl IV]	1F	0.74	21
8196.48	C III	43	0.37	33
8236.77	He II	5.9	0.72	19	1.81	15
8467.25	H I	P17	0.54	24
8502.48	H I	P16	0.39	30
8545.38	H I	P15	0.48	26
8598.39	H I	P14	0.77	26	0.65	22
8665.02	H I	P13	1.04	18
8703.25	N I	1	0.42	37
8750.47	H I	P12	1.02	16	1.04	24	1.13	17
8862.79	H I	P11	1.44	16
9014.91	H I	P10	1.78	13	1.69	22	1.75	16
9068.60	[S III]	1F	8.46	12	14.67	20	20.74	15
9229.01	H I	P9	1.97	13	1.97	13	3.06	15

NOTE.—“*” indicates that this emission line is blended with nearby ones. The total flux of a blend is indicated in the first listed line. “:” indicates uncertainties larger than 40%.

TABLE 3
EXTINCTION, TEMPERATURES AND DENSITIES

	Abell 46	Abell 63	Ou5
$c(\text{H}\beta)^{\text{a}}$	0.22 ± 0.08	0.55 ± 0.14	0.94 ± 0.10
$c(\text{H}\beta)^{\text{b}}$	$0.04^{+0.08}_{-0.04}$	0.38 ± 0.11	0.77 ± 0.14
$T_e([\text{O III}])$	12750 ± 200	8750 ± 950	11900 ± 500
$T_e([\text{O III}]^{\text{c}})$	12050 ± 200	7400 ± 550	10150 ± 300
$T_e([\text{N II}])$	>37000	>24000	20000 ± 8500
$T_e([\text{N II}]^{\text{c}})$	>30000	>22000	18800 ± 5000
$T_e(\text{He I } 5876/4471)$	1950^{+1050}_{-650}	1850^{+1300}_{-1000}	2800^{+4500}_{-1100}
$T_e(\text{He I } 6678/4471)$	2150^{+1850}_{-850}	2250^{+5000}_{-1250}	3200^{+5000}_{-1500}
$T_e(\text{Balmer jump})$	1150 ± 550
$T_e(\text{O II } 4089/4649)$	800^{+2800}_{-800}	...	$<1000:$
$T_e(\text{O II } V1/F1)$	4300 ± 100	4525 ± 125	5020 ± 360
$n_e([\text{S II}])$	340^{+570}_{-220}	600^{+2100}_{-450}	150^{+300}_{-100}
$n_e([\text{O II}])$	2750^{+880}_{-660}	2600^{+2500}_{-1300}	1200^{+550}_{-350}
$n_e([\text{Ar IV}])$	$<220:$...	300^{+800}_{-200}
$n_e(\text{CELS, adopted})$	1590 ± 600	1560^{+2000}_{-1100}	560^{+550}_{-300}
$n_e(\text{O II})$	2960	1940	3900

NOTE.—Temperatures are in units of Kelvin, and densities in cm^{-3} . “:” indicates uncertain values.

^aAssuming $T_e=12500$ K and $n_e=1000$ cm^{-3} .

^bAssuming $T_e=1000$ K and $n_e=1000$ cm^{-3} .

^cAfter correction for the estimated contribution of recombination to the auroral lines (see text and Table 6).

TABLE 4
 ATOMIC DATASET USED FOR COLLISIONALLY EXCITED LINES

Ion	Transition probabilities	Collisional strengths
N ⁺	Froese Fischer & Tachiev (2004) ^a	Tayal (2011)
O ⁺	Froese Fischer & Tachiev (2004)	Kisielius et al. (2009)
O ²⁺	Froese Fischer & Tachiev (2004) ^a	Storey et al. (2014)
Ne ²⁺	Galavis et al. (1997)	McLaughlin & Bell (2000)
S ⁺	Podobedova et al. (2009)	Tayal & Zatsarinny (2010)
S ²⁺	Podobedova et al. (2009)	Tayal & Gupta (1999)
Cl ²⁺	Mendoza (1983)	Butler & Zeippen (1989)
Cl ³⁺	Kaufman & Sugar (1986)	Galavís et al. (1995)
	Mendoza & Zeippen (1982a)	
	Ellis & Martinson (1984)	
Ar ²⁺	Mendoza (1983)	Galavís et al. (1995)
	Kaufman & Sugar (1986)	
Ar ³⁺	Mendoza & Zeippen (1982b)	Ramsbottom & Bell (1997)
Ar ⁴⁺	Mendoza & Zeippen (1982a)	Galavís et al. (1995)
	Kaufman & Sugar (1986)	
	LaJohn & Luke (1993)	

^aAdopting the A-values of Storey & Zeippen (2000) results in negligible changes in our T_e and abundances calculations.

TABLE 5
 ATOMIC DATASET USED FOR RECOMBINATION LINES

Ion	Recombination coefficients
H ⁺	Storey & Hummer (1995)
He ⁺	Porter et al. (2012, 2013)
He ²⁺	Storey & Hummer (1995)
C ²⁺	Davey et al. (2000)
O ²⁺	Storey (1994)
N ²⁺	Fang et al. (2011, 2013)

TABLE 6
 PERCENTUAL CONTRIBUTION OF RECOMBINATION TO SELECTED CELLS

Line	Abell 46	Abell 63	Ou5
[N II] 5755	13	9	8
[O II] 7320,7330	100	56	100
[O III] 4363	14	43	34

TABLE 7
IONIC ABUNDANCES AND *adf*s

Ion	Abell 46		Abell 63		Ou5	
	corrected ^a		corrected ^a		corrected ^a	
He ⁺	11.15±0.02	11.15±0.02	11.16±0.02	11.15±0.03	11.14±0.03	11.14±0.02
He ²⁺	10.35±0.01	10.35±0.01	10.76±0.01	10.75±0.03	10.78±0.01	10.77±0.01
C ²⁺ (ORLs)	9.81±0.02	9.81±0.02	9.57±0.06	9.57±0.06	9.70±0.05	9.70±0.05
N ⁺	5.72±0.04	5.78±0.04	6.26 ^{+0.15} _{-0.13}	6.48 ^{+0.14} _{-0.09}	6.32±0.05	6.49±0.05
O ⁺ (CELs)	6.83±0.05	6.92±0.05	7.18 ^{+0.29} _{-0.22}	7.55 ^{+0.22} _{-0.18}	6.97±0.09	7.24±0.07
O ⁺ (ORLs)	8.68±0.07	8.66±0.07
<i>adf</i> (O ⁺)	51	26
O ²⁺ (CELs)	7.77±0.02	7.85±0.02	8.17 ^{+0.18} _{-0.14}	8.46 ^{+0.16} _{-0.11}	8.05±0.06	8.26±0.05
O ²⁺ (ORLs)	9.93±0.04	9.93±0.04	9.36 ^{+0.18} _{-0.20}	9.36 ^{+0.18} _{-0.20}	10.01±0.08	10.01±0.08
<i>adf</i> (O ²⁺)	145	120	15	8	91	56
Ne ²⁺	7.25±0.03	7.34±0.03	7.70 ^{+0.22} _{-0.18}	8.05 ^{+0.20} _{-0.15}	7.61±0.08	7.87±0.05
S ⁺	4.81±0.09	4.86±0.08	4.80±0.24	5.01 ^{+0.18} _{-0.16}	5.17±0.07	5.32±0.06
S ²⁺	5.90±0.05	5.95±0.05	6.47±0.13	6.63±0.13	6.35±0.08	6.48±0.07
Ar ²⁺	5.48±0.04	5.53±0.04	6.03 ^{+0.15} _{-0.12}	6.23 ^{+0.14} _{-0.11}	5.88±0.05	6.03±0.05
Ar ³⁺	5.16±0.05	5.24±0.06	5.72±0.08	5.94±0.06
Ar ⁴⁺	4.48 ^{+0.27} _{-0.38}	4.66 ^{+0.20} _{-0.30}
Cl ²⁺	4.68 ^{+0.15} _{-0.20}	4.87 ^{+0.17} _{-0.19}
Cl ³⁺	4.57±0.10	4.72±0.10

NOTE.—Abundances are indicated in the usual notation as $\log(X^{i+}/H^+)+12$.

^aAfter removal of the estimated contribution of recombination to CELs (see text).

TABLE 8
TOTAL ABUNDANCES

Element	Abell 46		Abell 63		Ow5	
		corrected ^a		corrected ^a		corrected ^a
He	11.21 ± 0.01	11.22 ± 0.01	11.31 ± 0.02	11.30 ± 0.02	11.30 ± 0.05	11.29 ± 0.05
N	6.72 ± 0.05	6.77 ± 0.05	7.31 ^{+0.15} _{-0.11}	7.46 ± 0.11	7.46 ± 0.05	7.58 ± 0.05
O	7.85 ± 0.02	7.93 ± 0.02	8.30 ^{+0.20} _{-0.15}	8.59 ^{+0.16} _{-0.12}	8.18 ± 0.06	8.40 ± 0.05
Ne	7.29 ± 0.03	7.38 ± 0.03	7.78 ^{+0.22} _{-0.18}	8.14 ^{+0.19} _{-0.15}	7.70 ^{+0.08} _{-0.06}	7.96 ± 0.05
S	6.15 ± 0.05	6.19 ± 0.05	6.75 ± 0.13	6.89 ± 0.12	6.69 ± 0.08	6.81 ± 0.07
Ar	5.67 ± 0.04	5.72 ± 0.04	6.28 ^{+0.14} _{-0.12}	6.46 ± 0.12	6.15 ± 0.05	6.29 ± 0.05
Cl	5.02 ^{+0.15} _{-0.20}	5.20 ^{+0.17} _{-0.20}

NOTE.—All abundances are from CELs except for He. They are indicated as log(X/H)+12.

^aAfter removal of the estimated contribution of recombination to CELs (see text and Table 6).